Novel Peptides Selected to Bind Vascular Endothelial Growth Factor Target the Receptor-Binding Site

Wayne J. Fairbrother,[‡] Hans W. Christinger,[‡] Andrea G. Cochran,[‡] Germaine Fuh,[‡] Christopher J. Keenan,[‡] Clifford Quan,[§] Stephanie K. Shriver,[‡] Jeffrey Y. K. Tom,[§] James A. Wells,[‡,||] and Brian C. Cunningham*[,‡,||,]

Departments of Protein Engineering and Bioorganic Chemistry, Genentech, Inc., 1 DNA Way, South San Francisco, California 94080

Received August 11, 1998; Revised Manuscript Received October 20, 1998

ABSTRACT: Peptides that inhibit binding of vascular endothelial growth factor (VEGF) to its receptors, KDR and Flt-1, have been produced using phage display. Libraries of short disulfide-constrained peptides yielded three distinct classes of peptides that bind to the receptor-binding domain of VEGF with micromolar affinities. The highest affinity peptide was also shown to antagonize VEGF-induced proliferation of primary human umbilical vascular endothelial cells. The peptides bind to a region of VEGF known to contain the contact surface for Flt-1 and the functional determinants for KDR binding. This suggests that the receptor-binding region of VEGF is a binding "hot spot" that is readily targeted by selected peptides and supports earlier assertions that phage-derived peptides frequently target protein−protein interaction sites. Such peptides may lead to the development of pharmacologically useful VEGF antagonists.

Vascular endothelial growth factor (VEGF)[1] is a primary modulator of vascular neogenesis, angiogenesis, and vessel permeability (*1*, *2*). VEGF contains two identical polypeptide chains that are linked covalently by a pair of disulfide bonds (*3*, *4*). The hormone exists as five isoforms having 121, 145, 165, 189, or 206 residues per monomer (*3*−*7*). The different isoforms share a common N-terminal receptor-binding domain of 115 residues/monomer, while the longer forms ($VEGF_{165}$, $VEGF_{189}$, and $VEGF_{206}$) have the same C-terminal 50 residues which constitute a heparin-binding domain (*8*, *9*). VEGF induces dimerization of the tyrosine kinase receptors KDR [kinase insert domain containing receptor (*10*, *11*)] or Flt-1 [*fms*-like tyrosine kinase-1 (*12*)], which stimulates mitogenesis of vascular endothelium (*13*, *14*) or organizational effects on the vasculature (*15*, *16*), respectively. Receptor dimerization occurs as a consequence of the symmetry of the VEGF molecule, which presents a pair of identical binding sites located at the two poles of the VEGF receptor-binding domain (*17*−*20*).

In addition to its normal physiological role, VEGF is associated with numerous pathogenic states, including cancer, rheumatoid arthritis, diabetic retinopathy and psoriasis; development of VEGF antagonists is therefore clinically attractive (*21*). Indeed, neutralizing monoclonal antibodies (*22*, *23*) and SELEX-derived RNA molecules (*24*) that target VEGF, suppress tumor growth that is dependent on vascularization of adjacent normal tissue (*25*). Humanized neutralizing antibodies have been shown to interact with VEGF near the KDR and Flt-1 binding sites (*18*, *26*), while the RNA inhibitors are thought to interact specifically with the heparin-binding domain (*9*, *24*).

Multicopy display of random peptides on f1 filamentous phage particles has allowed the efficient selection of novel peptide ligands (*27*). We have used this technique to identify small disulfide-constrained peptides that are capable of blocking the interaction of VEGF with its receptors. The peptides have substantially lower molecular weights than the previously identified antibody or RNA antagonists and bind independently of the heparin-binding domain to a region of the receptor-binding domain common among the VEGF isoforms found in vivo. The peptides are thus potentially useful leads for the further development of VEGF antagonist molecules.

MATERIALS AND METHODS

Expression and Purification of VEGF. The receptor-binding domain of human VEGF (residues 8−109; $VEGF_{8-109}$) was overexpressed in *Escherichia coli* inclusion bodies, purified, and refolded as described previously (*28*). For NMR experiments, ^{15}N-labeled $VEGF_{11-109}$ was overexpressed in *E. coli* as a His-tagged protein, purified, refolded, and cleaved specifically, as described (*29*). Both VEGF constructs used in the present study have been shown by phage ELISA to have KDR−IgG binding affinities equivalent to that of $VEGF_{1-109}$ (*18*).

Construction of Random Peptide Libraries. A Gene VIII phagemid vector (*30*) was used to create phagemid libraries for polyvalent display of random peptides. The vector encodes the stII signal sequence followed by the peptide, and a $(Gly)_3$−Ser−$(Gly)_3$−Ala spacer links the peptide to the N-terminus of the Gene VIII coat protein. All peptide

* To whom correspondence should be addressed. Fax: (650) 556-8824. E-mail: bcc@sunesis-pharma.com.

[‡] Department of Protein Engineering.

[§] Department of Bioorganic Chemistry.

[||] Present address: Sunesis Pharmaceuticals, Inc., 3696 Haven Ave., Suite C, Redwood City, CA 94063.

[1] Abbreviations: BSA, bovine serum albumin; DTT, dithiothreitol; Flt-1, *fms*-like tyrosine kinase-1; HUVEC, human umbilical vein endothelial cells; KDR, kinase insert domain-containing receptor; VEGF, vascular endothelial growth factor.

10.1021/bi981931e CCC: $15.00
Published on Web 12/04/1998

Library A

X_7-C-X_4-C-X_7

X_7-C-X_5-C-X_6

X_6-C-X_6-C-X_6

X_6-C-X_7-C-X_5

X_5-C-X_8-C-X_5

X_5-C-X_9-C-X_4

X_4-C-X_{10}-C-X_4

Library B

X_4-C-X_2-GP-X_4-C-X_4

FIGURE 1: Twenty-residue peptide-phage libraries used for selection of VEGF-binding peptides.

sequences included a fixed pair of cysteine residues. Eight different libraries were constructed as described (*30*). Individual libraries had typical diversities of 5×10^8 and gave a combined diversity consisting of about 4×10^9 unique sequences.

Selection of VEGF-Binding Phage. A pool of seven $X_{(i)}CX_{(j)}CX_{(k)}$ libraries (library A) and a $X_4CX_2GPX_4CX_4$ library (library B) (Figure 1) were independently sorted for VEGF binders as follows: in the first and second rounds of sorting, biotinylated $VEGF_{8-109}$ (prepared by treatment of VEGF with 1.5 molar equivalents of NHS−SS−Biotin [sulfosuccinimidyl 2-(biotinamido) ethyl-1,3-dithiopropionate; Pierce]) was bound to neutravidin-coated Maxisorp plates (Nunc) and subsequently treated with Blocker Casein Buffer (Pierce). Phage libraries were added in blocking buffer and the plates were gently shaken for 1−2 h at room temperature. Unbound phage were rinsed away and the remaining bound phage were eluted by a 5 min treatment with 75 mM DTT, which cleaves the disulfide linker and releases immobilized VEGF. Eluted phage were then propagated in 20 volume equivalents of log phase XL-1 blue cells (Stratagene) for the next round of sorting. In the third and fourth rounds of sorting, conditions were modified to prevent the selection of casein or neutravidin binders. $VEGF_{8-109}$ was directly coated onto microtiter plates and blocked with 0.5% BSA. Bound phage were eluted with 10 mM HCl (in 100 mM NaCl and 0.3% BSA) instead of DTT because no reducible cross-link was present. The isolated phage were then neutralized with 0.05 vol of 1 M Tris (pH 8) and propagated for the next round of selection. Specific binding was monitored by measuring the number of phage that eluted from VEGF-coated microtiter plate wells versus the number eluted from identical wells that lacked the VEGF target.

Peptide Optimization by Soft Randomization. In contrast to the entirely random libraries (excluding the fixed cysteine residues) used to select the initial VEGF-binding peptides, libraries intended to evolve these sequences further were randomized only partially at each position. This process, referred to herein as "soft randomization", retains an overall sequence similarity to the parent peptide while introducing a fixed level of mutations from which improved sequences can be selected. Since the mutations occur over the entire sequence, soft randomization offers the advantage of enabling the selection of multiple cooperative mutations as well as simple point mutations. Additionally, the mutational frequency can be adjusted as necessary to accommodate different peptide lengths and library sizes. In this case, the mutagenesis primers were synthesized using an 80:7:7:7 mixture (i.e., 80% original base and ~7% each of the other three bases) for each base in the randomized codons. This translates to an amino acid mutation frequency of about 40% at each residue position in the peptide sequence. Libraries for soft randomization were prepared by site-directed mutagenesis of a Gene III monovalent phage-display vector (*31*), yielding 0.5×10^8, 0.75×10^8, and 2.0×10^8 independent peptide sequences for classes 1, 2, and 3 (see Results for definition of the peptide classes), respectively. The libraries were sorted against directly coated $VEGF_{8-109}$. Casein block was used for the initial two rounds of sorting, and BSA block was used in subsequent rounds. In each case, the phage-binding buffer used was the same as the blocking buffer. For the fourth and fifth rounds of sorting, an additional chasing step was employed to select for phagemid with slower off-rates. After rinsing away nonbinders, the plates were incubated for 3−16 h in the presence of 100 nM competing KDR to prevent the rebinding of dissociated phage. Another rinse step removed these phage before the bound phage were eluted with acid.

Peptide Optimization by Tailored Randomization. Libraries for tailored randomization were prepared by site-directed mutagenesis of the monovalent phage display vector described above. Mutagenesis primers were synthesized using equimolar mixtures of specific combinations of bases that were chosen to encode amino acids observed in the soft randomization selectants, while introducing as few additional residues as possible. The peptide-encoding portions of the oligonucleotides were GRG GAM CKG TGG TGC TTC SAM GGT CCT SKT GMA TGG GTG TGT KGG KDK VWW RDT (class 1), AGG GGC TGG GTG GAG ATC TGC GMA KCG GAC GWM WDS GGG MDW TGC STG AVT GRA SSA NNS (class 2), and VKC DDG NNS RMM TGC GAC RTT VHT RKA ATG TGG GWG TGG SAS TGC TTC GHA NKT KTM (class 3) (IUPAC nucleotide codes). These libraries contained 2.6×10^7, 1.4×10^7, and 1.3×10^8 independent clones for classes 1, 2, and 3, respectively. The first and second rounds of sorting were performed as described in the previous section. The third through seventh rounds of sorting were performed against progressively lower concentrations of solution-phase biotinylated $VEGF_{8-109}$. After 2 h, bound phage were captured with magnetic streptavidin beads (Strept. MagneSphere, Promega). The beads were rinsed 6 times, and the phage were eluted with DTT as described earlier.

Peptide Synthesis. Peptides were synthesized using standard 9-fluorenylmethoxycarbonyl (Fmoc) protocols, cleaved off the resin with 5% triisopropylsilane in trifluoroacetic acid (TFA), oxidized by potassium ferricyanide, and purified by reversed-phase HPLC. Masses of each peptide were verified by electrospray mass spectrometry.

Measurement of Binding Affinities. Affinities of peptides for VEGF were measured by BIAcore (BIAcore Inc.), using either a competitive binding assay or kinetic analysis of peptide binding directly to immobilized VEGF. For the competitive binding assay, monomeric human KDR (domains 1−3) and a heterodimeric VEGF variant with one binding site per dimer (hV-1) were expressed, refolded, and purified as described previously (*20*). Approximately 4000 refractive index units (RUs) of KDR(1−3) were coupled to a CM5

Class 1

A soft randomization

	library 1				5					10					15			18	
	nns	*nns*	*nns*	*nns*	*nns*	*nns*	*nns*	*nns*	*nns*	*nns*	*nns*	*nns*	*nns*	*nns*	*nns*	*nns*	*nns*	*nns*	
parent	G	E	R	W	C	F	D	G	P	L	T	W	V	C	G	E	E	S	
sort 5																			
481_2	G	E	R	W	C	F	E	G	P	V	A	W	V	C	G	E	E	N	***
481_6	G	E	R	W	C	F	E	G	P	V	A	W	V	C	G	E	D	S	*
481_4	G	E	R	W	C	F	D	G	P	R	A	W	V	C	G	E	D	S	*
481_5	G	E	R	W	C	F	D	G	P	R	A	W	V	C	G	W	E	I	*
481_1	G	E	R	W	C	F	E	G	P	L	A	W	V	C	G	E	E	S	*
sort 6																			
481_2	G	E	R	W	C	F	H	G	P	L	A	W	V	C	G	E	E	S	****
481_5	G	E	R	W	C	F	H	G	P	L	A	W	V	C	G	E	D	G	**
481_9	G	E	R	W	C	F	E	G	P	L	A	W	V	C	G	E	D	S	*
481_10	G	D	R	W	C	F	E	G	P	L	A	W	V	C	G	V	E	S	*
481_8	E	E	L	W	C	F	D	G	P	L	A	W	V	C	G	E	Q	S	*
481_1 (v106)	G	E	R	W	C	F	D	G	P	R	A	W	V	C	G	W	E	I	*
481_12	E	E	R	W	C	F	D	G	P	L	E	W	V	C	G	Y	D	S	*

B tailored randomization

	library *grg*	*gam*	*ckg*	W	C	F	*sam*	G	P	*skt*	*gma*	W	V	C	*kgg*	*kdk*	*vww*	*rdt*	
sort 5																			
499_1	E	E	L	W	C	F	D	G	P	R	A	W	V	C	G	Y	I	S	**
499_4	E	E	L	W	C	F	D	G	P	R	A	W	V	C	G	Y	L	K	*
499_6	E	E	L	W	C	F	D	G	P	R	A	W	V	C	G	Y	V	K	**
499_7	E	E	L	W	C	F	D	G	P	R	A	W	V	C	G	Y	V	G	**
499_9	E	D	L	W	C	F	D	G	P	R	A	W	V	C	G	Y	V	G	*
499_3	E	D	L	W	C	F	D	G	P	R	A	W	V	C	G	V	I	G	*
499_2	E	E	R	W	C	F	D	G	P	R	A	W	V	C	G				
sort 7																			
499_12	E	E	L	W	C	F	D	G	P	R	A	W	V	C	G	Y	I	K	*
499_13 (v127)	E	E	L	W	C	F	D	G	P	R	A	W	V	C	G	Y	V	K	**
499_18	E	E	L	W	C	F	D	G	P	R	A	W	V	C	G	Y	V	S	*
499_15	E	D	L	W	C	F	D	G	P	R	A	W	V	C	G	Y	V	G	*
499_14	E	E	L	W	C	F	D	G	P	R	A	W	V	C	G	W	Q	G	*

FIGURE 2: Class 1 of affinity optimized sequences that were selected from monovalent Gene III display libraries. (A) The selectant sequences from the soft randomization selection. Each residue of the parent sequence was soft randomized in the library as is designated by *nns*. The aligned sort 5 and 6 sequences are highlighted to show residues conserved with respect to the parent sequence. Clone identification numbers are shown and the peptide name given in parentheses for those that were synthesized and tested later. (B) The selected sequences from the tailored randomization selection. The tailored randomization codon scheme (IUPAC nucleotide code) used to prepare the random library is shown in italicized lower case. Asterisks (*) represent the number of individual clones identified for each amino acid sequence.

sensor chip (activated as the NHS ester). A fixed concentration of hV-1 (100 nM) was preincubated (30−120 min) with 3-fold serial dilutions of peptide. Samples were injected for 3 min at 10 μL/min. hV-1 alone was injected for comparison, before and after each peptide sample. The fractional binding of hV-1 in the presence and absence of peptide was calculated from the 3 min time points, and a four-parameter curve-fitting program (*32*) was used to compute IC_{50} values. For kinetic measurements, $VEGF_{8-109}$ (1500 RUs) was coupled to the sensor chip as described for KDR(1−3). Two-fold serial dilutions of peptide were injected at a flow rate of 20 μL/min. The observed binding profiles were analyzed by BIAevaluation 3.0 software using the simultaneous association and dissociation 1:1 Langmuir fitting routine.

Measurement of Biological Activity. Primary human umbilical vein endothelial cells (HUVEC) were prepared by passing them from two to five times in complete growth medium on dishes coated with attachment factors (Cell Systems). These cells (4000/well) were then seeded to microtiter plates and fasted in Dulbecco's modified minimal essential F-12 medium with 1% dialyzed fetal bovine serum for 24 h. Mixtures of 200 pM $VEGF_{1-165}$ with serial additions of test peptide were dispensed to microtiter wells coated with HUVE cells. The cells were cultured for an additional 24 h and exposed to [^{3}H]thymidine (0.5 mCi/well; Amersham) for 10 h. After washing the cells, the incorporated radiolabel was quantitated with a microplate scintillation counter (Packard).

NMR Analysis. All peptide and protein spectra were acquired on a Bruker AMX-500 spectrometer, equipped with a Bruker 5 mm inverse triple-resonance probe with three-axis gradient coils. Peptides v107 (∼2.5 mg) and v108 (∼2.0 mg) were dissolved in 380 μL of 90% H_2O/10% D_2O at pH 6.0 and 5.6, respectively, for structural characterization by

NMR spectroscopy. In addition to high-resolution one-dimensional ^{1}H NMR spectra, the following homonuclear two-dimensional (2D) NMR spectra were recorded at 10 or 20 °C using standard pulse sequences and phase cycling (*33*): 2QF−COSY, TOCSY, NOESY, and ROESY. Solvent suppression was achieved using pulsed field gradients for either coherence selection (*34*) or excitation sculpting (*35*). The TOCSY spectra were acquired using a 100 ms "clean" DIPSI-2rc isotropic mixing sequence (*36*). The NOESY spectra were acquired with mixing times of 350 ms, and the ROESY spectra were acquired with mixing times of 175 ms and a spin-lock field strength of 4 kHz. Vicinal $^3J_{HN-H\alpha}$ coupling constants were measured directly from high digital-resolution 2QF−COSY spectra. All spectra were processed and analyzed on Silicon Graphics workstations using the program FELIX (Molecular Simulations, Inc.). Resonance assignments were obtained using standard methods from the above 2D spectra (*37*).

Two-dimensional ^{1}H-^{15}N HSQC spectra of uniformly ^{15}N-labeled $VEGF_{11-109}$ were acquired in the presence and absence of selected peptides at 35 and 45 °C; solvent suppresion was achieved using the water "flip-back" method (*38*). Cross-peaks from the free $VEGF_{11-109}$ spectra were deemed to have been perturbed by peptide binding if no corresponding cross-peaks could be identified, at both temperatures, within approximately half a line width in the spectra of the $VEGF_{11-109}$/peptide complex samples. Each VEGF dimer binds two peptide molecules. The $VEGF_{11-109}$/peptide complex samples were thus made by addition of an approximately 2-fold molar excess of peptide to ∼0.4 mM protein (VEGF dimer) solutions (25 mM sodium phosphate and 50 mM NaCl, pH 7.0). In the case of v107 and v108, the peptides were concentrated such that addition of ∼50 μL of peptide solution to 450 μL of protein solution gave the desired stoichiometry; peptide concentrations were determined spectrophotometrically using calculated (*39, 40*) molar extinction coefficients ϵ_{280} = 11 500 and 7 090, respectively. For peptide v106, which is insoluble at millimolar concentrations, ∼1.5 mg of peptide was lyophilized and added directly to the protein sample; excess insoluble peptide was removed by centrifugation.

RESULTS

Selection of VEGF-Binding Peptides. Seven random disulfide-constrained peptide libraries of the form $X_{(i)}CX_{(j)}CX_{(k)}$, with j values ranging from 4 to 10 and $i + j + k = 18$ were generated (*30*) and pooled to produce library A (Figure 1). Additionally, a library of the form $X_4CX_2GPX_4CX_4$, designed to incorporate a type I β-turn within the disulfide loop as observed in the bound conformation of a peptide agonist of the erythropoeitin receptor (*27, 41*), was included as library B. These peptides were displayed as N-terminal fusions linked through a glycine-rich spacer sequence to the multicopy Gene VIII phage coat protein. After four rounds of sorting, a 6000−19000-fold increase in binding to immobilized $VEGF_{8-109}$ was observed relative to the background phage binding. Sequencing of representitive clones yielded a single consensus sequence for library B (GERWCFDGPLTWVCGEES; referred to hereafter as class 1) and two predominant sequences for library A (RGWVEICVADDNGMCVTEAQ, class 2; and GWDECDVARMWEWECFAGV, class 3).

Phage ELISA (*42*) experiments showed that the binding of these phage clones to VEGF could be blocked by KDR, indicating that they were potential antagonists (data not shown). Library A also yielded two selectants with cysteine residues in addition to the fixed pair. However, these sequences were not selected when the pool was displayed in a low-copy format on Gene III, suggesting that they were relatively weak binders or perhaps dependent on the formation of dimers (data not shown).

Initial Optimization of Peptides by Soft Randomization. An analysis by phage ELISA indicated that the selected sequences had only weak affinities for VEGF (K_d > 10 μM). However, the size of the original libraries was only a small fraction of the number of sequences possible for peptides of this length, so the peptides were further optimized using the monovalent phage display method (*31, 43*). Because the important binding determinants in the selected peptides were unknown and potentially cooperative, we employed a "soft" randomization strategy that retains a high percentage of the original amino acids but introduces diversity by spiking the codons with an equimolar ratio of the other three bases (see Materials and Methods).

Selectants in the libraries demonstrated strong binding to VEGF by the second round of sorting; bound phage titers were 12000−140000-fold higher than background levels after five rounds of sorting. After six rounds of sorting, phage ELISA experiments yielded IC_{50} values in the ranges 0.6−6.6, 0.6−1.7, and 0.3−1.3 μM, for the class 1, 2, and 3 selectants, respectively. Most of the sequences of the resulting clones were unique (Figures 2A, 3A, and 4A) and showed residues either being conserved, mutated to a new consensus, or partially mutated to a variety of different amino acids. These data suggest which residues were important in the original peptide, which changes might further improve binding, and which are simply tolerated but unimportant for binding. Not suprisingly, the cysteine residues were found to be conserved in all three classes, indicating that the disulfide constraints were criticial for affinity. Additionally, for the class 1 selectants, there was strong conservation of the Gly-Pro motif within the disulfide loop and the residues immediately neighboring the cysteines (Figure 2A). For the class 2 selectants, the six N-terminal residues were absolutely conserved, along with two other residues within the disulfide loop (D10 and G13). Finally, for the class 3 selectants, there were five residues in the C-terminal half of the disulfide loop that were very highly conserved. Examples of new highly selected mutations are T11A for class 1, V8E/A, N12Y/F, M14R/I/Q, and V16L for class 2, and A17V/E, G18S/R, and V19F/L for class 3. In contrast, the C-terminal residue Q20 in the class 2 peptide is an example of an apparently unimportant position; a variety of substitutions occur with frequencies near the theoretical mutation rate.

Binding Analysis of Soft Randomization Peptides. Representative peptides were synthesized to confirm that they could bind VEGF independently of fusion to the phage coat proteins. Class 1 (v106), class 2 (v108), and class 3 (v107) peptides blocked binding of a monomeric form of KDR to a heterodimeric form of $VEGF_{8-109}$ that has a single receptor-binding site per heterodimer [hV-1 (*20*)]; IC_{50} values were 7.0, 2.2, and 0.7 μM, respectively (Table 1). These values correlated well with the affinities of the respective phage for $VEGF_{8-109}$, indicating that the presentation on phage was

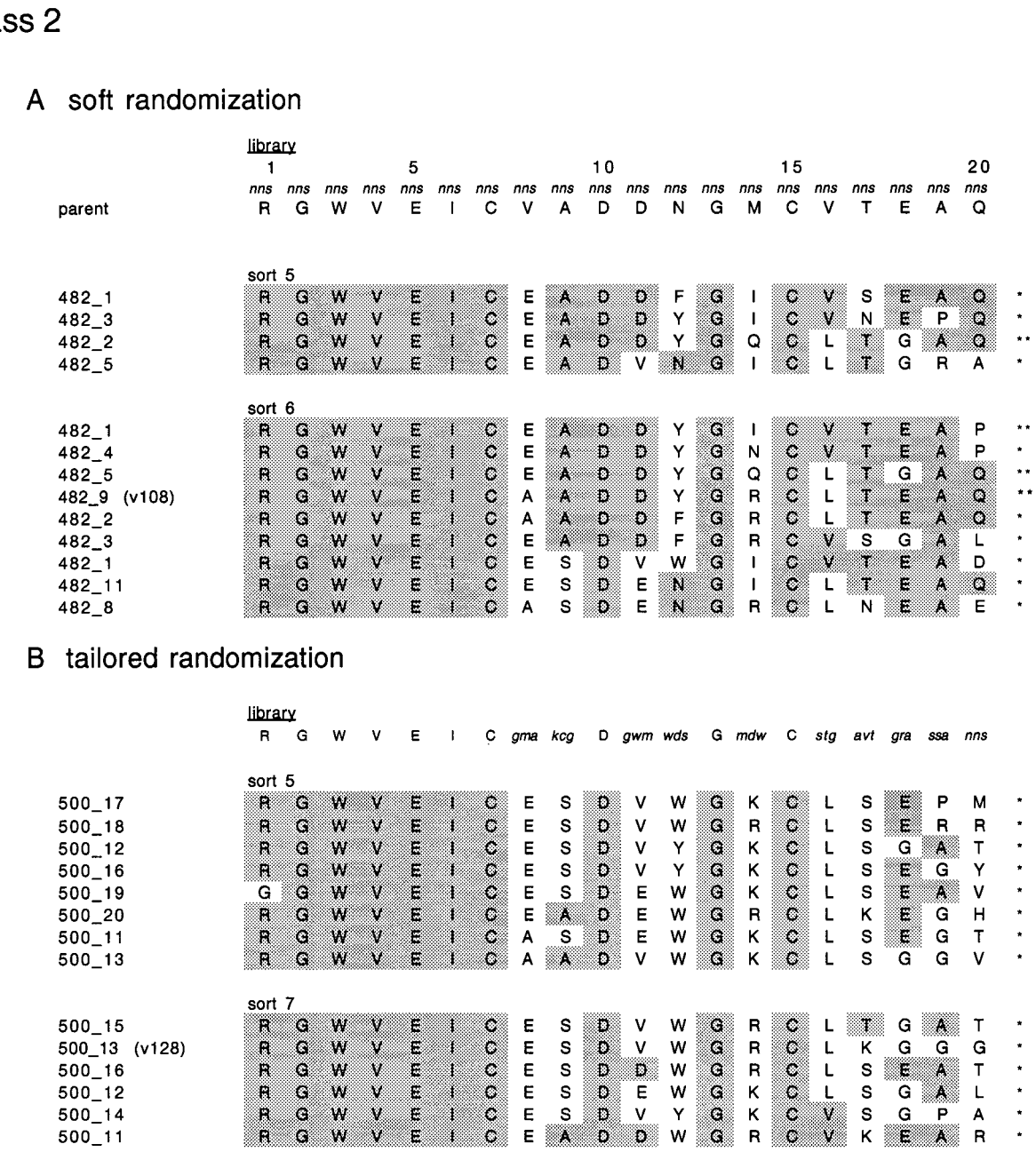

FIGURE 3: Class 2 of affinity optimized sequences that were selected from monovalent Gene III display libraries. Panels A and B are as described for Figure 2.

not contributing significantly to the affinity of the peptides (data not shown). Competitive ELISAs showed that all three peptide classes bind a common region on the VEGF molecule (Figure 5).

Final Optimization of Peptides by Tailored Randomization. A final optimization strategy was used in which limited randomizations were "tailored" for each peptide class. These libraries included primarily the mixture of residues that were selected from the soft randomization. For example, R, L, and V were selected at position 10 in the class 1 peptide (Figure 2A). In this case, a S(G/C):K(G/T):T codon, chosen to minimize unwanted substitutions, gave a mix of R, L, V, or G residues at this position. The calculated diversity possible for the chosen substitutions was 5×10^5, 4×10^6, and 8×10^8 for the class 1, 2, and 3 peptides, respectively. Synergistic improvements should be selected more efficiently because all possible combinations of the favored residues can be represented in the libraries. The library sizes for classes 1 and 2 were larger than the theoretical number of sequences while that for class 3 was only ~6-fold smaller (see Materials and Methods).

Robust phagemid binding of the tailored libraries to immobilized $VEGF_{8-109}$ occurred by the second round of selection (5000−17000-fold above background). The third through seventh rounds of sorting used a more stringent solution-based technique (see Materials and Methods) in which the VEGF concentration was progressively lowered from 50 to 1 nM; these concentrations still allowed 12−500-fold greater binding than background.

Sequence analysis of the selectants generally gave a clear yet different consensus from the soft randomization method. Tailored randomization of the class 1 peptides yielded substitutions G1E, R3L, L10R, T11A, E16Y, and E17V (Figure 2B); only T11A among these was preferred in the

Class 3

A soft randomization

	library																		
	1				5					10					15				19
	nns	*nns*	*nns*	*nns*	*nns*	*nns*	*nns*	*nns*	*nns*	*nns*	*nns*	*nns*	*nns*	*nns*	*nns*	*nns*	*nns*	*nns*	*nns*	
parent	G	W	D	E	C	D	V	A	R	M	W	E	W	E	C	F	A	G	V	
sort 5																				
485_1	G	Y	D	E	C	D	V	A	R	M	W	E	W	E	C	F	V	E	F	*
485_2	V	W	D	E	C	D	V	A	V	M	W	E	W	E	C	F	V	S	F	**
485_3	G	G	D	E	C	D	V	A	R	M	W	V	W	E	C	F	V	R	F	*
485_4	G	W	D	E	C	D	V	A	R	M	W	E	W	H	C	F	V	G	F	*
485_6	G	W	D	E	C	D	V	A	R	M	W	E	W	E	C	F	V	S	F	*
sort 6																				
485A_1	G	W	Q	E	C	D	V	A	R	M	W	E	W	E	C	F	V	S	F	*
485A_3	D	W	D	A	C	D	V	H	R	M	W	E	W	E	C	F	V	S	F	*
485A_4	V	W	D	E	C	D	V	A	V	M	W	E	W	E	C	F	V	S	F	**
485A_2	G	R	A	N	C	D	V	A	V	M	W	E	W	E	C	F	V	G	T	**
485R_3 (v107)	G	G	N	E	C	D	I	A	R	M	W	E	W	E	C	F	E	R	L	*
485R_4	S	W	D	E	C	D	V	T	R	M	W	E	W	E	C	F	E	R	L	*
485R_1	G	G	D	E	C	D	I	A	R	M	W	E	W	E	C	F	A	S	L	*
485R_2	R	E	G	A	C	D	V	A	R	M	W	E	W	E	C	F	A	F	V	*

B tailored randomization

	library																		
	vkc	*ddg*	*nns*	*rmm*	C	D	*rtt*	*vht*	*rka*	M	W	*gwg*	W	*sas*	C	F	*gha*	*nkt*	*ktm*	
sort 5																				
501_21	G	G	S	N	C	D	I	H	V	M	W	E	W	E	C	F	E	R	L	**
501_26	G	G	A	N	C	D	I	H	V	M	W	E	W	E	C	F	E	R	L	*
501_23	G	E	A	N	C	D	I	H	V	M	W	E	W	E	C	F	E	R	L	*
501_22	V	E	P	N	C	D	I	H	V	M	W	E	W	E	C	F	E	R	L	**
501_27	V	G	P	N	C	D	I	H	V	M	W	E	W	E	C	F	E	L	L	*
501_29	R	E	P	N	C	D	I	H	V	M	W	E	W	E	C	F	E	R	L	***
sort 7																				
501_17 (v114)	V	E	P	N	C	D	I	H	V	M	W	E	W	E	C	F	E	R	L	*****
501_22	R	E	P	N	C	D	I	H	V	M	W	E	W	E	C	F	E	R	L	*
501_21	G	E	A	N	C	D	I	H	V	M	W	E	W	E	C	F	E	R	L	*
501_23	G	E	V	N	C	D	I	H	V	M	W	E	W	E	C	F	E	R	L	*

FIGURE 4: Class 3 of affinity optimized sequences that were selected from monovalent Gene III display libraries. Panels A and B are as described for Figure 2.

soft randomization. For the class 2 peptides V8E, A9S, D11V, and N12W (Figure 3B), which occurred together in only one clone from the soft randomization, was the clear consensus from the tailored randomization. Likewise, in the class 3 sequence E4N, A8H, R9V, A17E, G18R, and V19L were strongly selected (Figure 4B).

Binding Analysis of Tailored Randomization Peptides. Representative peptides from the tailored randomization selectants were synthesized for analysis. The class 1 consensus peptide inhibited KDR binding with an IC_{50} of 10 μM (v127, Table 1). In this case, no improvement in binding was observed relative to the soft randomization selectant (v106, Table 1).

For class 2, the four C-terminal residues were omitted because structural data suggested that they were unimportant for VEGF binding (*44*). This conclusion is consistent with the poor consensus found in this region (Figure 3) and was confirmed by synthesis of a truncated 16 residue peptide that bound only 2-fold more weakly (v113, Table 1) than the 20 residue parent peptide (v108, Table 1). Introducing the substitutions selected in the tailored randomization step improved the affinity of the 16 residue peptide by ~4-fold (v128a, Table 1).

The class 3 consensus peptide was the best inhibitor identified in this study; the tailored optimization gave a 3-fold improvement in IC_{50} (v114, Table 1) relative to the soft randomization selectant (v107). Additionally, direct binding measurements to immobilized $VEGF_{8-109}$ showed a 7-fold slower off-rate (0.023 versus 0.16 s^{-1}) and a 5-fold tighter calculated binding constant for v114 relative to v107 (0.11 versus 0.53 μM).

Biological Activity. Since v114 was the highest affinity peptide isolated, its ability to block $VEGF_{1-165}$-induced proliferation of HUVE primary cell cultures was tested. As expected, the change in VEGF isoform from the heterodimeric variant hV-1 to wild-type $VEGF_{1-165}$ did not affect peptide binding as measured in the BIAcore-based competition assay (Table 1). The peptide blocked [^{3}H]-thymidine incorporation with an IC_{50} of 9.6 μM (Figure 6). The 27-fold increase in IC_{50} in this assay may have a number of causes, including a low receptor occupancy requirement for stimulating mitogenesis, cellular localization effects caused by the heparin-binding domain of $VEGF_{1-165}$, or potential losses of the peptide due to the extreme conditions

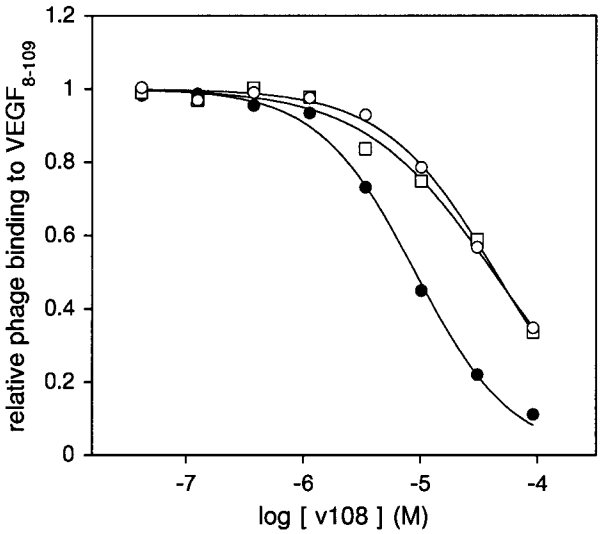

FIGURE 5: Competitive displacement of phagemid with the class 2 peptide v108. The displacement of phagemid displaying either the class 1 v106 sequence (○), the class 2 v108 sequence (●), or the class 3 v107 sequence (□) by the class 2 peptide v108. The data are consistent with the class 2 binding epitope overlapping the binding epitopes of both the class 1 and class 3 peptides.

Table 1: Measurements of IC_{50} Values for Synthetic Peptides

peptide	sequence	IC_{50} (μM)[a]	
	Class 1		
v106	GERWCFDGPRAWVCGWEI-NH_2* [b]	7.0 ± 0.9[c]	
v127	EELWCFDGPRAWVCGYVK-NH_2**	10.0	
	Class 2		
v108	RGWVEICAADDYGRCLTEAQ-NH_2*	2.2 ± 0.1	
v113	RGWVEICAADDYGRCL-NH_2*	4.0 ± 0.1	
v128a	RGWVEICESDVWGRCL-NH_2**	1.1	
	Class 3		
v107	GGNECDIARMWEWECFERL-NH_2*	0.70 ± 0.06	
v114	VEPNCDIHVMWEWECFERL-NH_2**	0.22	(0.35)[d]

[a] The IC_{50} values are the concentrations of peptide that resulted in blocking of 50% of a $VEGF_{8-109}$ variant (hV-1) binding to KDR(1−3) using a BIAcore based assay (see Materials and Methods). [b] (*) Peptides derived from sequences identified in the soft randomization selection, (**) peptides derived from sequences identified in the tailored randomization selection (Figures 2−4). [c] Values with uncertainties reported result from duplicate measurements. [d] The number in parentheses was determined identically except $VEGF_{1-165}$ was used in place of hV-1.

of this assay (see Materials and Methods). Lack of v114 inhibition of proliferation induced by an unrelated growth factor, aFGF, demonstrated that the blocked proliferation was not a general toxicity effect (data not shown).

NMR Structural Analysis. To better understand how the peptides bind to VEGF, the conformational preferences in aqueous solution of representative peptides were investigated by NMR spectroscopy. Phage-displayed peptide libraries have previously yielded a 14 residue peptide with a well-defined solution structure (*30*). Peptides v106, v108, and v107 were selected as representatives of classes 1, 2, and 3, respectively. The class 1 peptide v106 was found to be highly insoluble in water in the pH range tested (2.3−7.5), making structural characterization by NMR impossible. Peptides v108 and v107, on the other hand, were sufficiently soluble to allow complete ^1H resonance assignments (assignments are listed in Supporting Information).

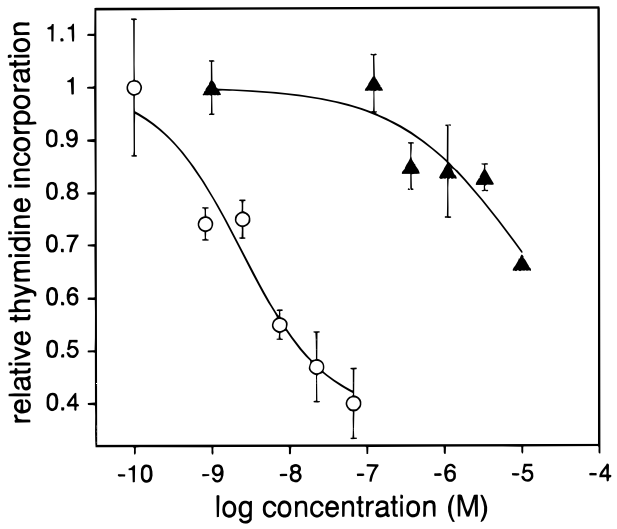

FIGURE 6: Inhibition of VEGF-induced HUVEC proliferation by the class 3 peptide v114. Each point on the graph represents the average of triplicate measurements and is shown with a one standard deviation error bar. The IC_{50} for the inhibition by v114 (▲) was 9.6 μM, while that measured for a potent mAb [A.4.6.1 (*52*)] (○) was 2.3 nM.

In the case of v108, only intraresidue and sequential correlations were observed in the NOESY and ROESY spectra, suggesting that under the solution conditions used (10 °C, pH 5.6) this peptide is essentially unstructured. All $^3J_{NH-H\alpha}$ coupling constants measured are between 6.1 and 8.0 Hz, consistent with averaging over many conformations.

In contrast to v108, peptide v107 has several $^3J_{NH-H\alpha}$ coupling constants less than 5.0 Hz, indicating the presence of helical turns, and a large number of medium and long-range NOE correlations. Unfortunately, the large number of cross-peaks gives rise to serious spectral overlap in the NOESY spectrum, making specific NOE assignment difficult. Distance geometry calculations using unambiguously assigned NOE-distance restraints together with ϕ dihedral angle restraints derived from the $^3J_{NH-H\alpha}$ coupling constants resulted in poorly converged structures with significant restraint violations, suggesting that the observed NOEs were not consistent with a single peptide conformation in solution. The large number of observed NOE correlations may result from either conformational exchange and/or aggregation (specific or nonspecific) in solution. Cross-peaks corresponding to E12, W13, and E14 are very broad in spectra acquired at 10 °C, but sharper in spectra acquired at 20 °C, consistent with this region of the peptide being involved in conformational exchange processes. The NMR data therefore indicate that peptide v107 populates multiple exchanging conformations in solution.

NMR Binding Analysis. The interaction sites for representative peptides on VEGF were characterized by mapping VEGF chemical shift perturbations upon peptide binding using 2D ^1H-^{15}N HSQC spectra of uniformly ^{15}N-labeled $VEGF_{11-109}$; the backbone resonance assignments for $VEGF_{11-109}$ have been reported previously (*29*). Chemical shifts of the protein amide resonances in these spectra result from their local magnetic-shielding environments, which depend on peptide bond anisotropy, aromatic ring current effects, electrostatic interactions, and hydrogen bonding. Peptide binding invariably causes local environmental changes

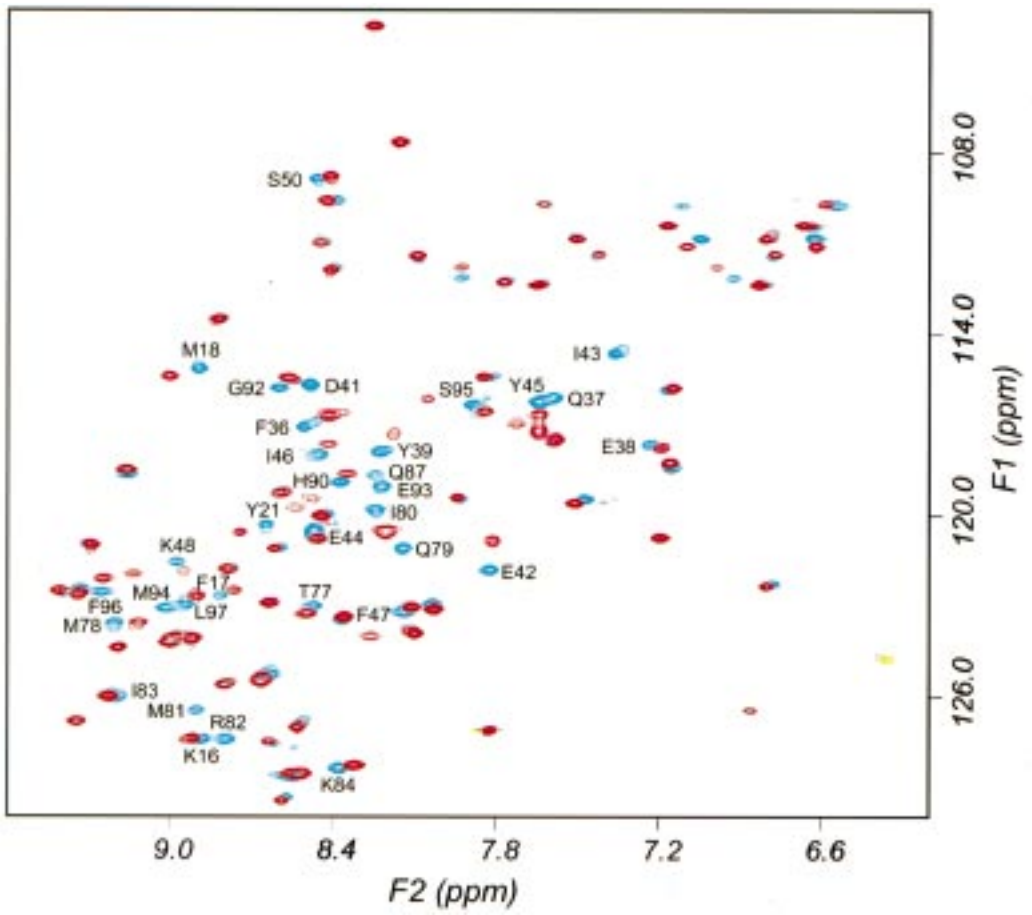

FIGURE 7: Superposition of 2D ^{1}H-^{15}N HSQC spectra of $VEGF_{11-109}$ in the absence (blue) and the presence (red) of the class 2 peptide v108. Cross-peaks in the free $VEGF_{11-109}$ spectrum that have experienced significant chemical shift changes upon binding peptide are labeled.

for nuclei in amino acids at the binding interface, resulting in observable chemical shift changes. In the absence of significant conformational change, these chemical shift perturbations provide a simple means to determine the interaction regions of both peptide−protein and protein−protein complexes (*45*, *46*). However, any conformational changes in the protein resulting from complex formation may cause additional chemical shift perturbations. Typically, the chemical shift effects extend slightly beyond the direct contact surface (*45*).

A superposition of HSQC spectra of $VEGF_{11-109}$ in the absence and the presence of class 2 peptide v108 is shown in Figure 7. The locations of residues with cross-peaks that experience significant chemical shift changes upon binding peptide (Table 2) are mapped onto a ribbon diagram of the $VEGF_{8-109}$ structure (*18*) in Figure 8B. Control experiments with peptides that do not interact with VEGF resulted in no detectable chemical shift changes upon addition to $VEGF_{11-109}$ (data not shown). The deduced peptide-binding region, which comprises residues at one end of the β-sheet of one monomer and residues from helix α-1 of the other monomer, includes residues that were previously identified as important for both KDR and Flt-1 binding (*18*−*20*) and for binding of neutralizing antibodies (*18, 26*).

Similar experiments were carried out for representative peptides from class 1 (v106) and class 3 (v107) (data not shown). VEGF residues whose chemical shifts were perturbed upon binding the peptides are summarized in Table 2; the locations of these residues on the VEGF structure are indicated in Figure 8, panels A and C, respectively. The three peptides appear to bind to distinct but overlapping regions of VEGF.

Table 2: Summary of VEGF Residues Whose Chemical Shifts Change upon Peptide Binding

secondary structure[a]	peptide		
	class 1 (v106)	class 2 (v108)	class 3 (v107)
α1	15−24	16−18, 21	16−24
α1-β1	26		25, 26
β1	32, 34		
α2	35, 36	36−39	
α2-β2		41−45	43
β2	46−48	46−48	47−48
β3		50	50−52
β3-β4	64		64, 65
β4	67		66−68
β5	81−84	77−84	79−83
β5-β6	86	86, 87	86
β6	90, 92−93	90, 92−97	
β7			103−105

[a] The residues are grouped according to their secondary structure location as defined by Muller et al. (*51*)

DISCUSSION

Phage display of unbiased peptide libraries has been used to identify three classes of small disulfide-constrained peptides that bind VEGF. Interestingly, competition binding experiments show that the peptides also inhibit the binding

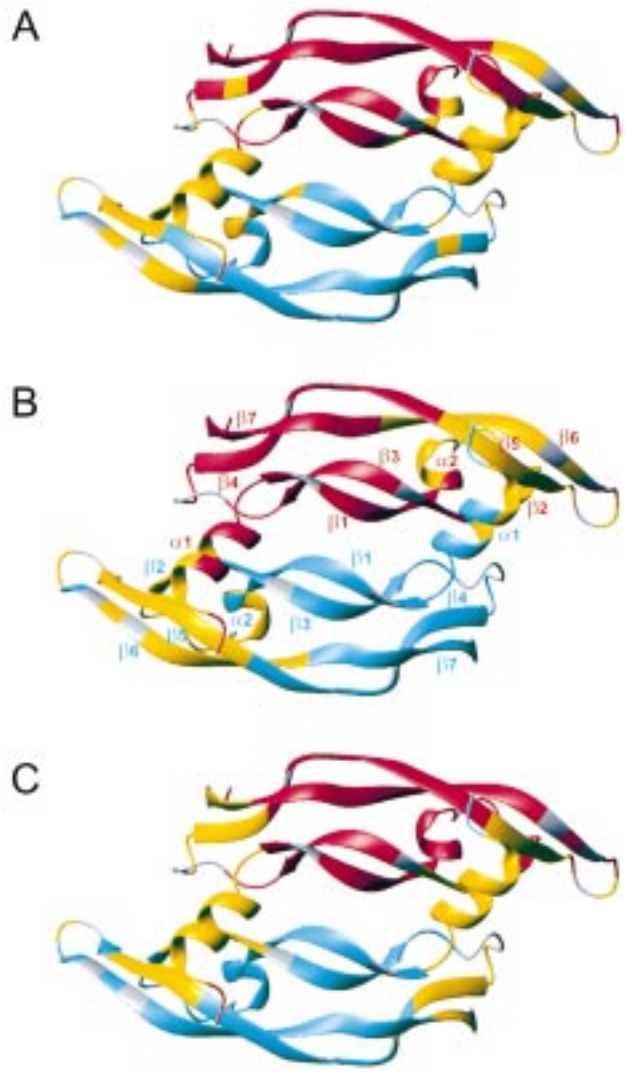

FIGURE 8: Schematic representations of the $VEGF_{8-109}$ crystal structure illustrating the locations of residues experiencing peptide binding induced chemical shift changes for peptides v106 (A), v108 (B), and v107 (C). The two subunits that form the VEGF dimer are colored red and blue. The secondary structure elements are labeled according to Muller et al. (*51*). Those residues whose backbone ^1H-^{15}N cross-peaks shifted on formation of the peptide−protein complex are highlighted in yellow. Residues that could not be assigned in the ^1H-^{15}N HSQC spectra are colored gray. This figure was produced using the program MOLMOL (*53*).

of VEGF to KDR, with IC_{50} values in the range 0.2−10 μM (Table 1), despite the fact that no selection methods were used to target the KDR-binding site of VEGF. Similar results were reported recently by Lowman et al. (*30*), who identified peptides from phage-displayed peptide libraries that bound to IGF-binding protein-1 (IGFBP-1) and also inhibited the binding of IGFBP-1 to IGF-1.

NMR analysis of peptide binding to $VEGF_{11-109}$ indicates that the different classes of peptides bind to overlapping VEGF epitopes (Figure 8); in particular, the chemical shifts of residues 16−18, 21, 47−48, 81−83, and 86 were perturbed upon peptide binding in each case (Table 2). The NMR data are thus consistent with the observed competition of class 2 peptide v108 for the class 1 and 3 binding sites (Figure 5). Although the peptide binding epitopes are clearly overlapping, the NMR data also indicate that the three classes of peptides bind VEGF in distinct ways. For instance, the class 2 peptide v108 induces chemical shift changes for 14 residues that are not observed for the other peptides (Table 2). On the basis of the chemical shift analysis, peptide v108 interacts with VEGF via the α2−β2 loop region and β-strands β5 and β6, and potentially contacts residues 16−18 and 21 in helix α1 of the other monomer (Figure 8B). The X-ray crystal structure of the $VEGF_{8-109}$/v108 complex confirms this view of the v108-binding site; the peptide is observed to contact VEGF residues 17−18 of helix α1, 36, 38−42, and 47−48 in the α2−β2 loop region, 79−82 of β-strand β5, and 89−95 of β-strand β6 (*44*). In contrast to v108, the class 3 peptide v107 does not appear to interact with the α2−β2 loop or β-strand β6, but rather interacts more extensively with the other monomer. This is indicated by chemical shift perturbations for residues 64−68 and 103−105 as well as for the entire helix α1. The class 3 interaction region thus comprises helix α1 and β-strands β4 and β7 from one monomer and β-strands β2 and β5 from the other monomer (Table 2, Figure 8C). The class 1 peptide v106 binding region appears to have features in common with both the class 2 and 3 binding regions (Table 2, Figure 8A).

The three classes of peptides identified in the present study each have binding sites that overlap significantly with both receptor and antibody-binding sites. The KDR and Flt-1 receptor-binding sites on VEGF have been characterized previously through alanine-scanning mutagenesis (*17*, *18*, *20*). The KDR-binding site of VEGF includes residues from both monomers of the homodimer: the most important residues for KDR binding are 17 and 18 from helix α1, 43, 46, and 47 from the α2−β2 loop region, 64 from the β3−β4 loop, and 79 and 83−85 from β-strand β5 (*18*, *20*). A more detailed view of the Flt-2-binding site is available from a 1.7 Å resolution crystal structure of $VEGF_{8-109}$ in complex with domain 2 of the receptor: residues in contact with Flt-1_{D2} include 16−18, 21, 22, 25, and 27 from helix α1; 46−48 from β-strand β2; 61−63 and 65−66 from the β3−β4 loop; 79, 81, 85−86, 89, and 91 from β-strands β5 and β6 and the intervening turn; and 103−106 from β-strand 7 (*19*). In addition, a recent 2.4 Å resolution crystal structure of a complex between $VEGF_{8-109}$ and a humanized neutralizing antibody (A4.6.1) revealed contacts with helix α1 (residues 17 and 21), the α2−β2 loop region (residues 45 and 48), and β-strands β5 and β6 (residues 79, 81−84, and 86−93) (*26*). The binding epitope of a second KDR-blocking antibody (3.2E3.1.1), determined by alanine-scanning mutagenesis, includes helix α1 residues 18, 21, 22, and 25 (*18*). The significant degree of overlap between these receptor- and antibody-binding sites and the peptide-binding sites provides further support for the suggestion that peptides derived from phage display of peptide libraries frequently target protein−protein interaction sites (*27*, *30*, *41*, *47*). There are a number of different VEGF-binding modes possible for both protein and peptide ligands. In all cases, however, significant contacts appear to be made with the hydrophobic side chains of Phe17 and Met81, which form the nucleus of a solvent exposed hydrophobic patch that also includes Tyr21, Ile46, Ile83, and Ile91 (Figure 9).

The deconvolution of common structural features in different molecules that target the same protein-binding site has been used to develop small molecule drug candidates (*48*−*50*). In the present case, however, the class 2 and 3 peptides were found to have no definable structures in

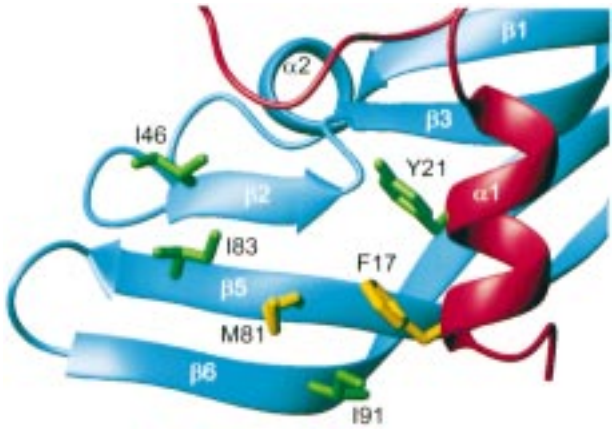

FIGURE 9: Schematic representation of the $VEGF_{8-109}$ crystal structure showing the location of a solvent exposed hydrophobic patch. The side chains of residues Phe17 and Met81 (yellow) appear to contact all protein and peptide ligands investigated to date; neighboring hydrophobic side chains are colored green. Ribbons corresponding to the two subunits from the VEGF dimer are colored red and blue. This figure was produced using the program MOLMOL (*53*).

solution (although the class 3 peptide v107 showed some evidence of helical turns); the class 1 peptide v106 was not sufficiently soluble for structural analysis. This is in contrast to the results of Lowman et al. (*30*), who found a highly structured peptide using similar phage display methods. Determination of the VEGF-bound structures of the de novo selected peptides may help deconvolute and identify critical binding interactions useful for designing smaller and more potent peptides or small molecules. The following paper in this issue presents such structural data for the $VEGF_{8-109}$/v108 complex (*44*); structural studies of other VEGF/peptide complexes are currently in progress.

ACKNOWLEDGMENT

We thank Warren L. Delano for writing the program used to select optimum codon usage for tailored randomization, and Mark Dennis, Henry B. Lowman, Gerald Nakamura, Nicholas J. Skelton, Melissa A. Starovasnik, and Abraham M. de Vos for valuable discussions and assistance.

SUPPORTING INFORMATION AVAILABLE

Two tables of the chemical shifts of v107 at pH 6.0, 10 °C, and v108 at pH 5.6, 10 °C (4 pages). See any current masthead page for ordering information.

REFERENCES

1. Dvorak, H. F., Brown, L. F., Detmar, M., and Dvorak, A. M. (1995) *Am. J. Pathol. 146*, 1029−1039.
2. Ferrara, N. (1995) *Breast Cancer Res. Treat. 36*, 127−137.
3. Leung, D. W., Cachianes, G., Kuang, W.-J., Goeddel, D. V., and Ferrara, N. (1989) *Science 246*, 1306−1309.
4. Keck, P. J., Hauser, S. D., Krivi, G., Sanzo, K., Warren, T., Feder, J., and Connolly, D. T. (1989) *Science 246*, 1309−1312.
5. Houck, K. A., Ferrara, N., Winer, J., Cachianes, G., Li, B., and Leung, D. W. (1991) *Mol. Endocrinol. 5*, 1806−1814.
6. Tischer, E., Mitchell, R., Hartman, T., Silva, M., Gospodarowicz, D., Fiddes, J. C., and Abraham, J. A. (1991) *J. Biol. Chem. 266*, 11947−11954.
7. Poltorak, Z., Cohen, T., Sivan, R., Kandelis, Y., Spira, G., Vlodavsky, I., Keshet, E., and Neufeld, G. (1997) *J. Biol. Chem. 272*, 7151−7158.
8. Keyt, B. A., Berleau, L. T., Nguyen, H. V., Chen, H., Heinsohn, H., Vandlen, R., and Ferrara, N. (1996) *J. Biol. Chem. 271*, 7788−7795.
9. Fairbrother, W. J., Champe, M. A., Christinger, H. W., Keyt, B. A., and Starovasnik, M. A. (1998) *Structure 6*, 637−648.
10. Terman, B. C., Dougher-Vermazen, M., Carrion, M. E., Dimitrov, D., Armellino, D. C., Gospodarowicz, D., and Böhlen, P. (1992) *Biochem. Biophys. Res. Commun. 187*, 1579−1586.
11. Millauer, B., Wizigmann-Voos, S., Schnurch, H., Martinez, R., Moller, N. P. H., Risau, W., and Ullrich, A. (1993) *Cell 72*, 835−846.
12. de Vries, C., Escobedo, J. A., Ueno, H., Houck, K., Ferrara, N., and Williams, L. T. (1992) *Science 255*, 989−991.
13. Shalaby, F., Rossant, J., Yamaguchi, T. P., Gertsenstein, M., Wu, X.-F., Breitman, M. L., and Schuh, A. C. (1995) *Nature 376*, 62−6.
14. Shalaby, F., Ho, J., Stanford, W. L., Fischer, K.-D., Schuh, A. C., Schwartz, L., Bernstein, A., and Rossant, J. (1997) *Cell 89*, 981−90.
15. Fong, G.-H., Rossant, J., Gertsenstein, M., and Breitman, M. L. (1995) *Nature 376*, 66−70.
16. Fong, G.-H., Klingensmith, J., Wood, C. R., Rossant, J., and Breitman, M. L. (1996) *Dev. Dyn. 207*, 1−10.
17. Keyt, B. A., Nguyen, H. V., Berleau, L. T., Duarte, C. M., Park, J., Chen, H., and Ferrara, N. (1996) *J. Biol. Chem. 271*, 5638−5646.
18. Muller, Y. A., Li, B., Christinger, H. W., Wells, J. A., Cunningham, B. A., and de Vos, A. M. (1997) *Proc. Nat. Acad. Sci. 94*, 7192−7197.
19. Wiesmann, C., Fuh, G., Christinger, H. W., Eigenbrot, C., Wells, J. A., and de Vos, A. M. (1997) *Cell 91*, 695−704.
20. Fuh, G., Li, B., Crowley, C., Cunningham, B. C., and Wells, J. A. (1998) *J. Biol. Chem. 273*, 11197−11204.
21. Folkman, J. (1995) *Nat. Med. 1*, 27−31.
22. Kim, K. J., Li, B., Houck, K., Winer, J., and Ferrara, N. (1992) *Growth Factors 7*, 53−64.
23. Kim, K. J., Li, B., Winer, J., Armanini, M., Gillett, N., Phillips, H. S., and Ferrara, N. (1993) *Nature 362*, 841−844.
24. Jellinek, D., Green, L. S., Bell, C., and Janjic, N. (1994) *Biochemistry 33*, 10450−10456.
25. Plate, K. H., Breier, G., and Risau, W. (1994) *Brain-Pathol. 4*, 207−218.
26. Muller, Y. A., Chen, Y., Christinger, H. W., Li, B., Cunningham, B. C., Lowman, H. B., and de Vos, A. M. (1998) *Structure 6*, 1153−1167.
27. Wrighton, N., Farrell, F., Chang, R., Kashyap, A., Barbone, F., Mulcahy, L., Johnson, D., Barrett, R., Jolliffe, L., and Dower, W. (1996) *Science 273*, 458−463.
28. Christinger, H. W., Muller, Y. A., Berleau, L. T., Keyt, B. A., Cunningham, B. C., Ferrara, N., and de Vos, A. M. (1996) *Proteins: Struct., Funct., Genet. 26*, 353−357.
29. Fairbrother, W. J., Champe, M. A., Christinger, H. W., Keyt, B. A., and Starovasnik, M. A. (1997) *Protein Sci. 6*, 2250−2260.
30. Lowman, H. B., Chen, Y. M., Skelton, N. J., Mortensen, D. L., Tomlinson, E. E., Sadick, M. D., Robinson, I. C. A. F., and Clark, R. G. (1998) *Biochemistry 37*, 8870−8878.
31. Bass, S. H., Greene, R., and Wells, J. A. (1990) *Proteins: Struct., Funct., Genet. 8*, 309−314.
32. Lowman, H. B. (1998) *Methods Mol. Biol. 87*, 249−264.
33. Cavanagh, J., Fairbrother, W. J., Palmer, A. G., III, and Skelton, N. J. (1995) *Protein NMR spectroscopy: principles and practice*, Academic Press, San Diego.
34. van Zijl, P. C. M., O'Neil-Johnson, M., Mori, S., and Hurd, R. E. (1995) *J. Magn. Reson., Ser. A, 113*, 265−270.
35. Hwang, T.-L., and Shaka, A. J. (1995) *J. Magn. Reson., Ser. A, 112*, 275−279.
36. Cavanagh, J., and Rance, M. (1992) *J. Magn. Reson. 96*, 670−678.
37. Wüthrich, K. (1986) *NMR of Proteins and Nucleic Acids*, John Wiley & Sons, Inc., New York.
38. Grzesiek, S., and Bax, A. (1993) *J. Am. Chem. Soc. 115*, 12593−12594.

39. Edelhoch, H. (1967) *Biochemistry 6*, 1948−1954.
40. Gill, S. C., and von Hippel, P. H. (1989) *Anal. Biochem. 182*, 319−326.
41. Livnah, O., Stura, E. A., Johnson, D. L., Middleton, S. A., Mulcahy, L. S., Wrightson, N. C., Dower, W. J., Jolliffe, L. K., and Wilson, I. A. (1996) *Science 273*, 464−471.
42. Cunningham, B. C., Lowe, D. G., Li, B., Bennett, B. D., and Wells, J. A. (1994) *EMBO J. 13*, 2508−2515.
43. Lowman, H. B., and Wells, J. A. (1993) *J. Mol. Biol.* 234, 564−578.
44. Wiesmann, C., Christinger, H. W., Cochran, A. G., Cunningham, B. C., Fairbrother, W. J., Keenan, C. J., Meng, G., and de Vos, A. M. (1998) *Biochemistry 38*, 17765−17772.
45. Spitzfaden, C., Weber, H.-P., Braun, W., Kallen, J., Wider, G., Widmer, H., Walkinshaw, M. D., and Wüthrich, K. (1992) *FEBS Lett. 300*, 291−300.
46. Chen, Y., Reizer, J., Saier, M. H., Jr., Fairbrother, W. J., and Wright, P. E. (1993) *Biochemistry 32*, 32−37.
47. Kay, B. K., Adey, N. B., He, Y.-S., Manfredi, J. P., Mataragnon, A. H., and Fowlkes, D. M. (1993) *Gene 128*, 59−65.
48. McDowell, R. S., Gadek, T. R., Barker, P. L., Burdick, D. J., Chan, K. S., Quan, C. L., Skelton, N., Struble, M., Thorsett, E. D., Tischler, M., Tom, J. Y. K., Webb, T. R., and Burnier, J. P. (1994) *J. Am. Chem. Soc. 116*, 5069−5076.
49. McDowell, R. S., Blackburn, B. K., Gadek, T. R., McGee, L. R., Rawson, T., Reynolds, M. E., Robarge, K. D., Somers, T. C., Thorsett, E. D., Tischler, M., Webb, R. R., II, and Venuti, M. C. (1994) *J. Am. Chem. Soc. 116*, 5077−5083.
50. McDowell, R. S., Elias, K. A., Stanley, M. S., Burdick, D. J., Burnier, J. P., Chan, K. S., Fairbrother, W. J., Hammonds, R. G., Ingle, G. S., Jacobsen, N. E., Mortensen, D. L., Rawson, T. E., Won, W. B., Clark, R. G., and Somers, T. C. (1995) *Proc. Natl. Acad. Sci. U.S.A. 92*, 11165−11169.
51. Muller, Y. A., Christinger, H. W., Keyt, B. A., and de Vos, A. M. (1997) *Structure 5*, 1325−1338.
52. Presta, L. G., Chen, H., O'Connor, S. J., Chisholm, V., Meng, Y. G., Krummen, L., Winkler, M., and Ferrara, N. (1997) *Cancer Res. 57*, 4593−4599.
53. Koradi, R., Billeter, M., and Wüthrich, K. (1996) *J. Mol. Graphics 14*, 51−55.

BI981931E